Probing the Dynamics of CO2 and CH4 within the Porous Zirconium Terephthalate UiO-66(Zr): A Synergic Combination of Neutron Scattering Measurements and Molecular Simulations

ARTICLE *in* CHEMISTRY - A EUROPEAN JOURNAL · JUNE 2011

Impact Factor: 5.73 · DOI: 10.1002/chem.201003596 · Source: PubMed

CHEMISTRY
A EUROPEAN JOURNAL

DOI: 10.1002/chem.201003596

Probing the Dynamics of CO_2 and CH_4 within the Porous Zirconium Terephthalate UiO-66(Zr): A Synergic Combination of Neutron Scattering Measurements and Molecular Simulations

Qingyuan Yang,[a, d] Hervé Jobic,*[b] Fabrice Salles,[a] Daniil Kolokolov,[b, e] Vincent Guillerm,[c] Christian Serre,[c] and Guillaume Maurin*[a]

Abstract: Quasi-elastic neutron scattering (QENS) measurements combined with molecular dynamics (MD) simulations were conducted to deeply understand the concentration dependence of the self- and transport diffusivities of CH_4 and CO_2, respectively, in the humidity-resistant metal–organic framework UiO-66(Zr). The QENS measurements show that the self-diffusivity profile for CH_4 exhibits a maximum, while the transport diffusivity for CO_2 increases continuously at the loadings explored in this study. Our MD simulations can reproduce fairly well both the magnitude and the concentration dependence of each measured diffusivity. The flexibility of the framework implemented by deriving a new forcefield for UiO-66(Zr) has a significant impact on the diffusivity of the two species. Methane diffuses faster than CO_2 over a broad range of loading, and this is in contrast to zeolites with narrow windows, for which opposite trends were observed. Further analysis of the MD trajectories indicates that the global microscopic diffusion mechanism involves a combination of intracage motions and jump sequences between tetrahedral and octahedral cages.

Keywords: diffusion · metal–organic frameworks · molecular dynamics · neutron diffraction

Introduction

Over the past twenty years, remarkable progress has been achieved in the synthesis and characterization of metal–organic frameworks (MOFs).[1,2] Because of their high specific surface areas, large pore volumes, and ease of modulating functionalities in the pore walls, a large number of studies have been conducted to explore the performance of these materials as energy carriers for H_2[3] and containers for CH_4 storage.[4] Furthermore, the urgent environmental and economical problems have galvanized researchers to seek novel competitive MOF materials able to efficiently capture CO_2. Interestingly, in 2005 very high CO_2 uptake was reported for MOF-177 solid,[5a] exceeding the capacity of any available commercial porous adsorbents including activated carbon and zeolites. Later, the performance of this material was surpassed by those of the MOF-type solid MIL-101 (MIL: Materials of Institute Lavoisier) under similar conditions.[5b] More recently, two novel crystal sponges MOF-200 and MOF-210 were found to be able to capture 1.6 times more CO_2 than MOF-177, and their ultrahigh surface areas were claimed to be near the ultimate adsorption limit for porous materials.[5c] All of these breakthrough studies greatly stimulate the MOF community to directly probe the performance of hybrid porous materials for selectively adsorbing CO_2 from mixtures with CH_4, both experimentally[6] and theoretically.[7] Such CO_2/CH_4 separation is of great interest in pressure swing adsorption (PSA) applications, where conventional zeolites such as the NaX-type faujasites are usually considered,[8] although these materials have the disadvantage of requiring high-temperature treatment for their regeneration.

Among this class of MOF materials, the zirconium terephthalate solid denoted as UiO-66(Zr) (UiO: University of Oslo)[9] was selected in this study. Its hydroxylated structure (see Figure 1) is built up from inorganic nodes $Zr_6O_4(OH)_4(CO_2)_{12}$ linked with terephthalate ligands in a such a way to

[a] Dr. Q. Yang, Dr. F. Salles, Dr. G. Maurin
Institut Charles Gerhardt Montpellier (UMR 5253)
Université Montpellier II, CNRS, ENSCM
Place E. Bataillon, 34095 Montpellier CEDEX 05 (France)
Fax: (+33) 491-637-111
E-mail: guillaume.maurin@univ-montp2.fr

[b] Dr. H. Jobic, Dr. D. Kolokolov
Institut de Recherches sur la Catalyse et l'Environnement de Lyon
Université de Lyon, CNRS
2. Av. A. Einstein, 69626 Villeurbanne (France)
E-mail: herve.jobic@ircelyon.univ-lyon1.fr

[c] V. Guillerm, Dr. C. Serre
Institut Lavoisier, UMR CNRS 8180, Université de Versailles
78035 Versailles (France)

[d] Dr. Q. Yang
Department of Chemical Engineering
Beijing University of Chemical Technology
Beijing (P. R. China)

[e] Dr. D. Kolokolov
Boreskov Institute of Catalysis
Siberian Branch of Russian Academy of Sciences
Prospekt Akademika Lavrentieva 5, Novosibirsk 630090 (Russia)

Supporting information for this article is available on the WWW under http://dx.doi.org/10.1002/chem.201003596.

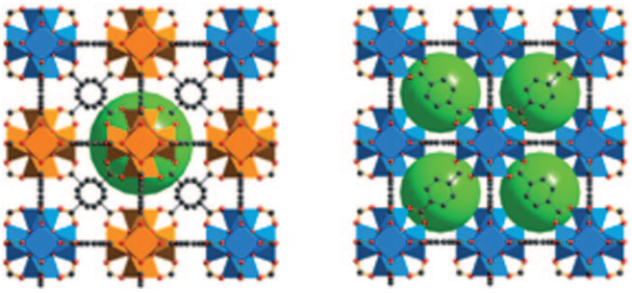

Figure 1. Schematic illustration of the UiO-66(Zr) structure. Left: octahedral cage; right: tetrahedral cages. Hydrogen atoms on the organic linkers were omitted for clarity. The large green spheres represent the void regions inside the cages (Zr polyhedra: yellow for octahedral cages, blue for tetrahedral cages; C, gray; O, red).

form an eight-coordinate environment around the Zr^{4+} centers. This leads to a 3D porous solid in which each centric octahedral cage is surrounded by eight corner tetrahedral cages (free diameters of ca. 11 and 8 Å for the two types of cages, respectively) connected through narrow windows (ca. 6 Å). This material shows very high thermal stability and remains unaltered on water adsorption/desorption cycles.[10a] Furthermore, we have evidenced from a thermodynamic point of view[10b] that this MOF-type material exhibits very encouraging properties for CO_2/CH_4 gas separation by combining good selectivity, very high working capacity, and potential regenerability under mild conditions, which make it an alternative to the conventional faujasite adsorbents used in PSA applications.

However, besides thermodynamics, the kinetic factor is a further basic property that can significantly affect the separation performance of an adsorbent. Hence, it is essential to gain insight into the dynamics of CO_2 and CH_4 within the UiO-66(Zr) MOF type structure. Up to now, compared to the adsorption investigations, only a few studies have been devoted to the diffusion of CO_2 and CH_4 in humidity-resistant MOF materials. Rankin et al.[11a] employed molecular dynamics (MD) simulations to predict the self- and transport diffusivities of several light gases including CO_2 and CH_4 in zeolitic imidazolate framework (ZIF) materials ZIF-68 and ZIF-70. Liu et al.[11b] and Sirjoosingh et al.[11c] studied the self-diffusivity of CO_2 in ZIF-68 and ZIF-69.[11c] More recently, Krishna et al.[11d] investigated the concentration dependence of the self- and Maxwell–Stefan diffusivities for CO_2 and CH_4 in MIL-47(V) and large-pore version of MIL-53(Cr), with emphasis on molecular clustering phenomena. In complement to these purely theoretical studies, we previously combined quasi-elastic neutron scattering (QENS) measurements with MD simulations to successfully address the loading dependence of the self- and transport diffusivities for CO_2 and CH_4 in MIL-47(V) and MIL-53(Cr) and further elucidate the diffusion mechanism within the pores of these materials.[12] In MIL-47(V), we evidenced that the CO_2 molecules do not behave like an ideal gas, and this leads to a thermodynamic correction factor of less than unity at low loading. By using this dual strategy, the work here aims at: 1) determining the loading dependence of the self- and transport diffusivities for CH_4 and CO_2, respectively, in the promising UiO-66(Zr) solid, 2) comparing profiles and absolute diffusivity values with those observed in the conventional faujasites (NaX) usually involved in PSA applications as well as in zeolites with narrow-window structure, 3) probing the impact of the framework flexibility on the diffusivity, and 4) further addressing the microscopic diffusion mechanism for both diffusive species through a detailed analysis of QENS spectra and MD runs.

Results and Discussion

Since scattering from CO_2 is weak, a deuterated analogue of UiO-66(Zr) was prepared to reduce scattering from the MOF framework. The synthesis was performed according to our previous procedure[10a] with deuterated instead of hydrogenated terephthalic acid as reactant.[13] To completely exclude the effect of residual water inside the pores on the dynamics of the guest molecules, the MOF material was initially fully activated in its dehydroxylated form prior to the QENS measurements by out-gassing the sample at 473 K. It was previously shown that the overall framework structure of the dehydroxylated version is indeed very similar to the hydroxylated structure shown in Figure 1, and both of them have the same arrangement of the two types of cages.[9] The only difference comes from the variation of the coordination number of the Zr center between the hydroxylated (8) and dehydroxylated forms (7). The QENS measurements were then carried out at 230 K on the time-of-flight spectrometer IN6 at the Institut Laue-Langevin, Grenoble, France, by using the procedure described in the Experimental Section to probe the self- and transport diffusivities of CH_4 and CO_2, respectively, as a function of the loading. These experimental findings were then complemented by MD simulations for exploring the microscopic diffusion mechanism.

Self-diffusivity of CH_4 in UiO-66(Zr): For methane, one follows the mobility of individual CH_4 molecules, since the scattering is dominated by the large incoherent cross section of hydrogen. Subtraction of the signal of empty UiO-66(Zr) does not modify the shape of the spectra, as the scattering from methane is large compared to that of the solid. The QENS spectra obtained for different loadings at 0.29 $Å^{-1}$ are shown in Figure 2. The broadening, and hence the diffusivity, increases up to a loading of 10.5 CH_4 per unit cell (u.c.) and then decreases (a plot of the width versus methane loading is presented in Figure S1 of the Supporting Information). Spectra obtained at different Q values could be fitted with a model consisting of isotropic diffusion, convoluted with isotropic rotation and with the instrumental resolution.

The self-diffusion coefficient D_s for methane was thus obtained,[14] and the resulting values are reported in Figure 3. As expected from the above QENS spectra, the D_s profile shows a nonmonotonic evolution, with the presence of a

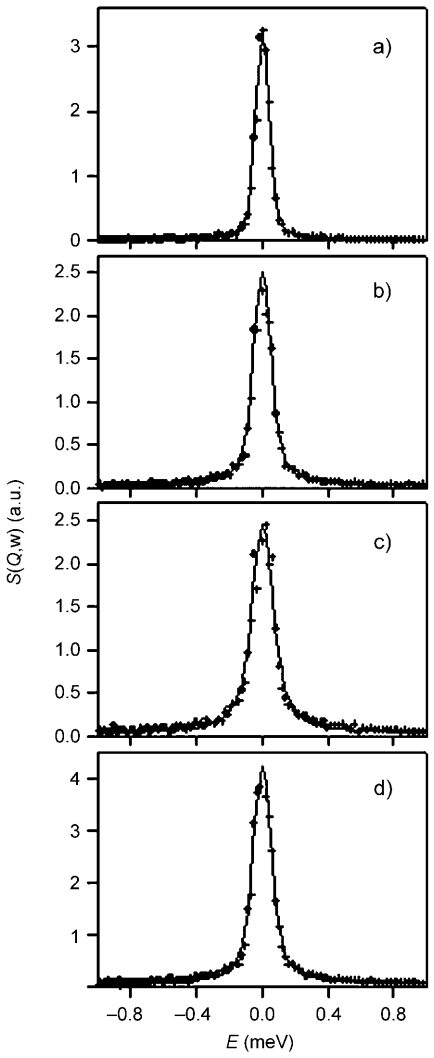

Figure 2. QENS spectra obtained at 230 K for methane in UiO-66(Zr), for increasing concentrations of CH_4 per u.c. a) 4.4, b) 8.4, c) 10.5, d) 16.5. The crosses correspond to the experimental points, and the solid lines to the calculated spectra ($Q = 0.29$ Å^{-1}).

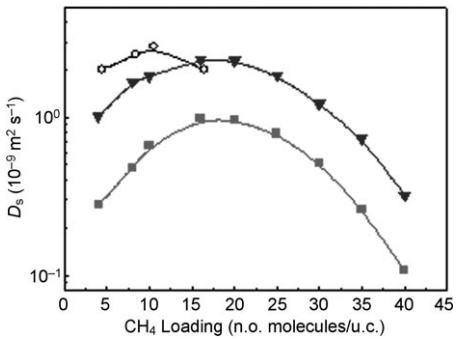

Figure 3. Evolution of self-diffusion coefficients as a function of the CH_4 loading in UiO-66(Zr) at 230 K: QENS (empty circles), simulations with rigid (filled squares) and flexible (filled triangles) framework.

maximum. Such concentration-dependent behavior was observed previously for CH_4 diffusing in various zeolites with narrow-window structure, including DDR, CHA, LTA, and ITQ-3,[15] which have similar topologies to UiO-66(Zr). Recently, this peculiar profile was also experimentally found for diffusion of CH_4 in faujasite NaY with large windows.[16a] The D_s value for CH_4 at the lowest loading of 4.4 CH_4/u.c. is about 2.0×10^{-9} m^2 s^{-1} (Figure 3). As shown in Table 1, this value is comparable to the QENS data reported for CH_4 in NaY[16a] under similar experimental conditions, and remains within the same order of magnitude as those measured by the pulsed-field gradient (PFG) NMR technique in NaX.[16b] Moreover, the thus-obtained D_s value is much higher than those for CH_4 in high-silica DDR, CHA, and LTA which were measured by the PFG NMR method.[16c]

To interpret the D_s profile at the microscopic level, complementary MD simulations were performed to investigate the dynamics of CH_4 in UiO-66(Zr). Briefly, these simulations were conducted at 230 K based on a model that only includes Lennard–Jones (LJ) interactions. CH_4 was represented by a neutral united atom model,[17a] while an atomistic representation was used to describe the dehydroxylated UiO-66(Zr) framework, by considering the crystalline structure previously solved by DFT calculations.[10a] The LJ potential parameters for the framework atoms were taken from the DREIDING forcefield.[17b] This whole forcefield was previously validated on the thermodynamic properties of UiO-66(Zr),[10b] and the whole set of potential parameters is summarized in the Supporting Information. The MD simulations were realized in the NVT ensemble by using the Nosé–Hoover thermostat, with a simulation box consisting

Table 1. Comparison of the self diffusivities of CH_4 and CO_2 in various nanoporous materials (here, the QENS and PFG NMR data are related to intracrystalline and to both intra- and intercrystalline diffusion processes respectively). The structural characteristics of these materials are given in Table S6.

Material	T [K]	$D_s(CH_4)$ [m^{2}s^{-1}]	Data type	Ref.
NaX	223	$(3.0–10.0)\times10^{-9}$	PFG NMR	–[16b]
NaY	200	$(5.3–7.9)\times10^{-9}$	QENS	–[16a]
DDR[a]	301	1.6×10^{-12}	PFG NMR	–[16c]
CHA[a]	301	1.1×10^{-11}	PFG NMR	–[16c]
LTA[a]	301	1.4×10^{-10}	PFG NMR	–[16c]
UiO-66(Zr)	230	$(2.0–2.8)\times10^{-9}$	QENS	this work
Material	**T [K]**	**$D_s(CO_2)$ [m^{2}s^{-1}]**	**Data type**	**Ref.**
NaX	300	$(0.7–9.0)\times10^{-10}$	simulation	–[8b]
DDR	300	$(0.1–1.0)\times10^{-9}$	simulation	–[15b]
MIL-47(V)	230	$(1.5–2.0)\times10^{-9}$	simulation	–[12b]
ZIF-68	300	$(1.5–8.0)\times10^{-10}$	simulation	–[11a]
ZIF-70	300	$(1.8–5.5)\times10^{-9}$	simulation	–[11a]
UiO-66(Zr)	230	$(2.4–6.7)\times10^{-10}$	simulation	this work
Material	**T [K]**	**$D_0(CO_2)$ [m^{2}s^{-1}]**	**Data type**	**Ref.**
NaX	300	$(0.2–10.0)\times10^{-9}$	QENS	–[8b]
MIL-47(V)	230	$(1.0–3.0)\times10^{-9}$	simulation	–[12b]
UiO-66(Zr)	230	$(2.2–5.6)\times10^{-10}$	simulation	this work
Materials	**T [K]**	**$D_t(CO_2)$ [m^{2}s^{-1}]**	**Data type**	**Ref.**
NaX	300	$(0.6–12.0)\times10^{-9}$	QENS	–[8b]
MIL-47(V)	230	$(0.8–2.8)\times10^{-8}$	QENS	–[12b]
MIL-53(Cr)	230	$(1.5–3.8)\times10^{-8}$	QENS	–[12c]
ZIF-68	300	$(0.12–4.0)\times10^{-9}$	simulation	–[11a]
ZIF-70	300	$(1.7–15.0)\times10^{-9}$	simulation	–[11a]
UiO-66(Zr)	230	$(0.8–9.5)\times10^{-9}$	QENS	this work

[a] Measured at 101.3 kPa.

of 18 unit cells of UiO-66(Zr) loaded with 72, 144, 180, and 288 CH_4 molecules to be consistent with the experimentally investigated loadings. In addition, five more CH_4 concentrations, corresponding to 360, 450, 540, 630, and 720 molecules, were also explored to span a wider range of loading. The MD runs were realized at each loading for 2×10^7 steps (i.e., 20 ns) with a time step of 1 fs. As a first step, the framework of the solid was kept fixed during the simulation, which has been commonly done in many theoretical studies for zeolites[15] and MOFs.[7] From the mean-square displacement (MSD) curves of the targeted molecules averaged over multiple time origins and five independent MD trajectories, it was then possible to extract D_s by using the Einstein relation. As shown in Figure 3, the simulated profile also shows a maximum at a CH_4 loading only slightly shifted compared to experiment (ca. 15 CH_4/u.c. versus 10.5 CH_4/u.c.). However, it is also observed that the simulations based on a rigid framework lead to a significant underestimation of the self-diffusion coefficients obtained from QENS measurements, especially at low loading.

Some recent MD simulations highlighted that the flexibility of the framework has a significant influence on the diffusion of guest species in MOFs[12,18] and zeolites,[19] particularly when the pore size of these solids is similar to the kinetic diameter of the diffusive species. Furthermore, as mentioned elsewhere,[20] the flexibility of the framework is known to have a profound effect on the intercage hopping process across the narrow windows when the guest molecules are strongly confined, for example, CH_4 in LTA,[19a] propane/propylene in CHA,[19b] and C_2H_6 in the MOF material Zn(tbip)[18b] with one-dimensional (1D) channel/window structure. For these reasons, MD simulations were also carried out with a flexible UiO-66(Zr) framework. To that end, the flexibility of this material was modeled by a fully bonded forcefield in which the metal–oxygen interactions were treated as covalent bonds. Preliminary MD simulations conducted in the NσT ensemble, where the shape and dimensions of the unit cell can vary, were carried out to derive this forcefield by closely matching 1) the unit cell parameters and 2) the equilibrium distances of various bond types of the dehydroxylated framework. The resulting force field and the set of parameters are described in the Supporting Information. Based on this derived flexible force field, the loading dependence of the self-diffusivity of CH_4 at 230 K in UiO-66(Zr) was then again simulated. As can be seen in Figure 3, while the D_s profile remains the same as those obtained with a rigid framework, and the maximum is reached for a similar CH_4 loading, the thus-simulated D_s values reproduce much better the QENS data. As a typical illustration, at the lowest loading (ca. 4 CH_4/u.c.), the simulated D_s values are 2.8×10^{-10} and 1.0×10^{-9} m^2s^{-1} for a rigid and a flexible framework, respectively, while the experimental value is 2.0×10^{-9} m^2s^{-1} Such observations demonstrate that considering a flexible UiO-66(Zr) framework leads to more realistic diffusivity values for CH_4, especially at lower loading, while it is not expected to modify the global diffusion mechanism as the trend for D_s is unchanged. In addition, we also ran the MD simulations at several temperatures for a loading of 4 CH_4/u.c., from which the activation energies can be calculated by using an Arrhenius equation. The calculated activation energies are 9.0 and 6.0 kJ mol^{-1} for the rigid and flexible cases, respectively. Indeed, a rigid lattice leads to more restriction on the motion of CH_4 molecules, consistent with slower diffusivity, as shown in Figure 3. This observation differs from our previous findings that show that the flexibility of the framework has only a negligible effect on the thermodynamic properties of this material.[10b] Indeed, it can be concluded that the UiO-66(Zr) behaves more like a "dynamic" framework when one probes the diffusion of the species trapped within its porosity.

To shed some light onto the microscopic diffusion mechanism, the MD trajectory for each CH_4 loading was carefully analyzed. From a visual inspection of these trajectories, it was observed that CH_4 diffuses either by intracage motions inside both types of cages or by jump sequences "tetrahedral cages–octahedral cages–tetrahedral cages", as illustrated in Figure 4a. Furthermore, the CH_4 molecules obey a 3D-type diffusion mechanism, consistent with the isotropic diffusion behavior evidenced from the fit of the QENS spectra. Moreover, the CH_4 molecules spend most of their time in the tetrahedral cages and quickly jump back or into another tetrahedral cage once they enter the octahedral cage. This dynamic behavior is mainly governed by energetic considera-

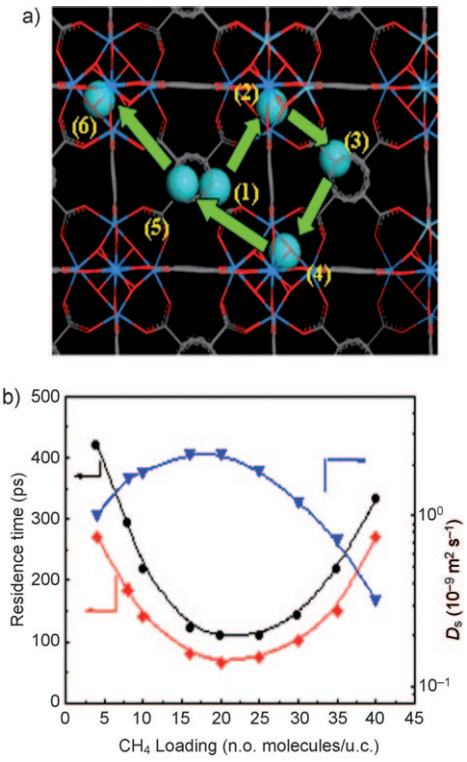

Figure 4. a) Typical illustration of the global diffusion mechanism in UiO-66(Zr) by following one targeted methane molecule at a loading of 4 CH_4/u.c. Positions 1–6 correspond to jump sequences of CH_4 observed during the MD trajectories. b) Residence-time profiles for CH_4 in the tetrahedral cages of UIO-66(Zr) at 230 K. Circles: rigid framework, diamonds: flexible framework, triangles: self-diffusivity simulated with a flexible framework.

tions. Indeed, the potential-energy surface experienced by a probe CH_4 molecule shows a deeper well consistent with the presence of tetrahedral cages (see Figure S7, Supporting Information).

Based on these observations, the microscopic picture of the diffusion can be further rationalized by the plot of the residence time for CH_4 inside the tetrahedral cages as a function of the loading. As can be observed in Figure 4b, the profile for the residence time obtained in both rigid and flexible frameworks is consistent with the trend observed for the self-diffusivity. At low loading, due to the confinement and energetic effect in the tetrahedral cages, the CH_4 molecules are preferentially adsorbed and mainly remain trapped inside these cages, which is consistent with long residence time and medium-range values of the self-diffusivity. As the loading increases, the additional CH_4 molecules present in the tetrahedral cages are involved in less favorable interactions with the pore wall and thus increase the net driving force to promote hopping of CH_4 towards the octahedral cages, which leads to a decrease of the residence time in the tetrahedral cages. When the CH_4 molecules reach the octahedral cages, they are subjected to less energetic interactions with the pore wall, as previously evidenced.[10b] Both factors lead to an increase of D_s in this range of loading, as shown in Figure 3. With a further increase in loading, the effect of steric hindrance becomes evident, and results in an increase of the residence time in the tetrahedral cages and a decrease in the self-diffusivity (see Figure 3). Figure 4b also shows that whatever the CH_4 loading, the residence times in the tetrahedral cages obtained when one uses a flexible framework are smaller than those calculated for the rigid case. This trend is consistent with the higher mobility of CH_4 observed in the flexible case, as already mentioned for other porous materials.[18,19]

Self-diffusivity of CO_2 in UiO-66(Zr): Due to the coherent scattering cross section of C and O atoms in CO_2 molecules, the mobility of individual CO_2 molecules cannot be extracted from QENS measurements. Indeed, Figure 5 only shows the predicted self-diffusion coefficient for CO_2 as a function of the loading at 230 K. As we have established above for CH_4 that the flexibility of the framework has a significant impact on the diffusivity in this material, the results shown in Figure 5 as well as the simulated corrected and transport diffusivities in the next section are reported from the MD runs with a flexible framework. Compared with the data reported in Figure 3, one observes that CO_2 diffuses more slowly than CH_4 over a broad range of loading, which is consistent with a longer residence time for CO_2 in the tetrahedral cages (see Figure 5) than those calculated for CH_4. In addition, the activation energy of 10.9 kJ mol^{-1} for CO_2 at the lowest loading of 7 CO_2/u.c. is higher than that estimated for CH_4 (6.0 kJ mol^{-1}), following the same trend than the adsorption enthalpy at low coverage previously estimated for both species (CO_2: −25.3 kJ mol^{-1}; CH_4: −18.8 kJ mol^{-1}).[10b] This trend can be also related to the higher mobility of CH_4. This slower diffusivity of CO_2 compared to CH_4 differs from

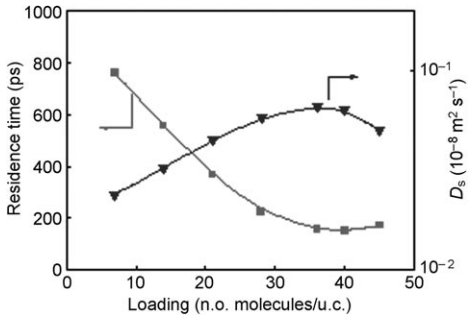

Figure 5. Simulated self-diffusivity (triangles) of CO_2 in UiO-66(Zr) at 230 K as a function of loading. The residence times (squares) for CO_2 molecules in the tetrahedral cages of UIO-66(Zr) are also shown.

the behavior usually observed in narrow-window zeolites (LTA, DDR, and CHA),[15b] where the opposite trend has been explained by the slender shape of CO_2 compared to CH_4. Figure 5 also indicates that the self-diffusion coefficients of CO_2 become larger than those of CH_4 at high loadings, which is consistent with the smaller residence time for CO_2 in the tetrahedral cages in this range of loading, as shown in Figures 4 and 5. This is caused by a more tight packing effect of CH_4 molecules at high loading compared to CO_2 and results in higher diffusivity of the latter.

This nonmonotonic variation of D_s of CO_2 presented in Figure 5 is similar to those previously predicted in ZIF-68 and ZIF-70 with cagelike structures,[11a] but is different from those in MIL-47(V),[12b] DDR,[15b] and NaX,[8b] which show a decreasing trend with increasing CO_2 loading. In addition, as can be seen from Table 1, the predicted D_s of CO_2 of $(2.4–6.7)\times10^{-10}$ m^{2}s^{-1} in UiO-66(Zr) at 230 K is comparable to those simulated in ZIF-68[12b] and NaX[8b] at 300 K, but almost one order of magnitude smaller than those in ZIF-70[11a] at 300 K and MIL-47(V)[12b] at 230 K and similar loadings as well as in DDR at 300 K.[15b] Here, such a D_s profile is explained by a microscopic diffusion mechanism similar to that detailed above for CH_4. Indeed, CO_2 also combines both intra- and intercage motions, whereby the tetrahedral–octahedral–tetrahedral cage-jump sequence is affected by the loading in the same way as for CH_4. This microscopic mechanism, which was also previously proposed to explain the same monotonic D_s profile for CO_2 in ZIF-68 and ZIF-70,[11a] differs from those invoked for DDR,[21] MIL-47(V),[12b] and NaX,[8b] wherein the steric effect causes a decreasing evolution of D_s as a function of loading.

Transport diffusivity of CO_2 in UiO-66(Zr): In contrast with CH_4, CO_2 is a totally coherent scatterer, so that the collective mobility is extracted from the QENS data. Subtraction of the contribution of empty UiO-66(Zr) creates negative peaks, as the Bragg intensity due to the solid is modified on adsorption. Spectra obtained at different CO_2 loadings are shown in Figure 6 for a Q value of 0.4 Å^{-1}. Since the signal from the solid is totally elastic, one can still measure the broadening due to CO_2, because it is larger than the instrumental resolution. The spectra could be fitted by an isotrop-

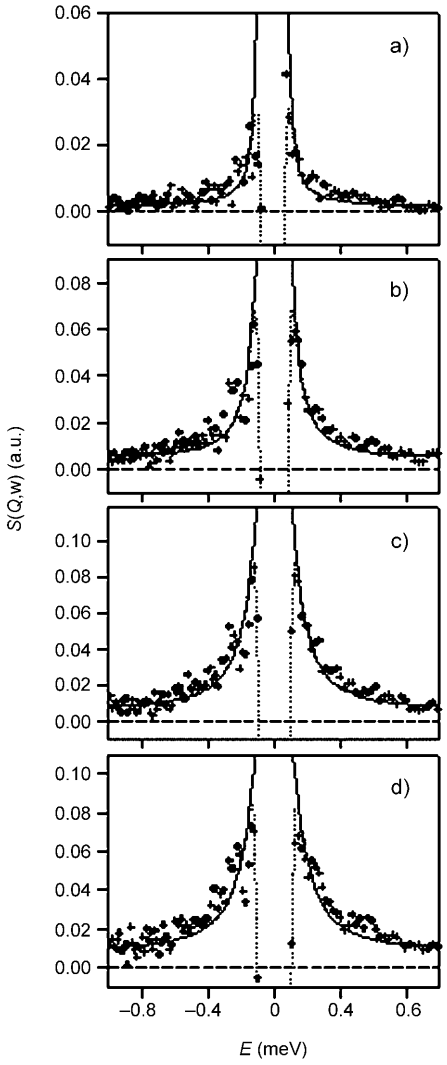

Figure 6. Comparison between experimental (crosses) and fitted (solid lines) QENS spectra obtained for CO_2 in UiO-66(Zr); the dotted lines indicate the negative elastic intensity due to UiO-66(Zr). The concentrations of CO_2 per u.c. are a) 6.9, b) 21.4, c) 35.7, and d) 38 ($Q = 0.4$ Å^{-1}).

ic translational motion alone, since rotation of this coherent scatterer is negligible at small Q values.[14] The broadening in Figure 6 increases continuously with increasing concentration, and no maximum is observed within the investigated loading range. It is the transport diffusivity of CO_2 which is obtained, as one probes the time evolution of the density fluctuations which occur at equilibrium.[14] The resulting experimental D_t values are reported in Figure 7.

One observes from Figure 7 a continuous increasing evolution of D_t with pore loading, consistent with the trends previously reported for CO_2 in zeolite-type materials such as NaY or NaX,[8b] as well as in MOF-type materials such as ZIF-68 and ZIF-70.[11a] The D_t values vary by almost one order of magnitude over the whole range of loading examined experimentally, in the range $(0.8–9.5)\times10^{-9}\,m^2s^{-1}$. These diffusion coefficients are smaller than those in MIL-47(V)[12b] and in MIL-53(Cr)[12c] for the same species at the same temperature and similar range of loading, while they

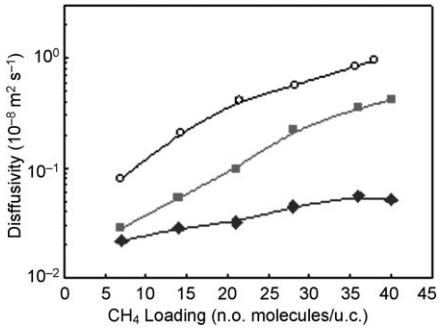

Figure 7. Evolution of the experimental transport diffusivity (D_t, circles) and the simulated corrected (D_0, diamonds) and transport (D_t, squares) diffusivities in UiO-66(Zr) at 230 K.

remain within the same range of those obtained in NaX at 300 K[8b] and predicted in both ZIF-68 and ZIF-70 at 300 K and similar loadings[11a] (see Table 1).

Molecular dynamics simulations were further performed at 230 K to help interpret the increasing profile for D_t obtained from QENS data and further elucidate the transport diffusion mechanism on the microscopic scale. The simulation box was again composed of 18 unit cells loaded with 126, 252, 378, 504, 648, and 720 CO_2, molecules, covering the experimentally explored loadings. The corrected diffusion coefficient D_0 was then calculated for each CO_2 loading by using the method previously reported.[15c] This approach is based on an Einstein relation that considers the MSD of the center of mass of the diffuse species (see Supporting Information for further details). One observes that D_0 does not remain constant in the explored concentration range, but shows an increasing profile with values varying by a factor of about 2.5 over the range of loading. This observation indicates that the profile for D_0 cannot be described by the so-called Darken approximation,[15c] which identifies the corrected diffusivity as a constant independent of loading. Such a simulated D_0 profile is similar to those previously reported in NaX[8b] and various MOFs,[11a,d] while it deviates from the decreasing trend observed in DDR and LTA.[15b] The resulting absolute values ranging from $2.2\times10^{-10}\,m^2s^{-1}$ to $5.6\times10^{-10}\,m^2s^{-1}$ are at least one order of magnitude lower than the data previously reported in NaX at 300 K[8b] while they are comparable with those previously predicted in MIL-47(V)[12b] (see Table 1).

The transport diffusivity was then calculated from D_0 by using Equation (1),

$$D_t(c) = D_0(c)\left(\frac{\partial \ln f}{\partial \ln c}\right) \quad (1)$$

in which the partial derivative involving the adsorbate concentration c and the bulk-phase fugacity f is known as the thermodynamic correction factor Γ. This derivative is fully defined once the adsorption isotherm is available. Thus, the flexible force field was first used to calculate the adsorption isotherm of CO_2 in UiO-66(Zr) at 230 K by means of grand

canonical Monte Carlo (GCMC) simulations (Figure S4 in Supporting Information), which was further fitted by using a dual-site Langmuir model. From the excellent agreement between the fitted and simulated isotherms, Γ values were then extracted as reported in Figure S5 of the Supporting Information. The D_t values calculated by using Equation (1) are reported as a function of CO_2 loading in Figure 7. The increasing profile of D_t is in good accordance with the experimental data. Furthermore, the experimental absolute values are only slightly underestimated. Finally, at the limit of zero concentration of the adsorbate, the three quantities D_s, D_t, and D_0 become almost equal, converging around $1.8\times10^{-10}\,m^2\,s^{-1}$, very similar to the experimental value for D_t ($2.1\times10^{-10}\,m^2\,s^{-1}$).

To clarify the microscopic mechanism for the corrected diffusivity, the probability density distributions of CO_2 within the pores of UiO-66(Zr) were calculated from the analysis of the configurations generated by MD runs at 230 K. The corresponding density plots of the center of mass (COM) of the adsorbed molecules at two loadings (7 CO_2/u.c. and 36 CO_2/u.c.) shown in Figure 8 were selected as typical cases. These snapshots first show that the CO_2 molecules remain preferentially located in the tetrahedral cages. Visual inspections of the trajectories generated from the MD simulations show for all loadings that the CO_2 molecules also obey a 3D-type diffusion mechanism in the same way as mentioned above for the self-diffusion behavior of CH_4. At low loading, the net motions of the COM of the CO_2 molecules mainly occur inside the tetrahedral cages, consistent with Figure 8a, which shows that the probability of finding the COM of the CO_2 molecules in the octahedral cages is low. When the loading increases, the displacements of the COM of the CO_2 molecules also involve jumps towards the octahedral cages, and thus higher diffusivity is favored. This behavior is again consistent with the 2D density plot in Figure 8b, which emphasizes a higher probability density in the octahedral cages compared to the low-loading situation. Indeed, the global dynamics is thus a combination of intracage motions and intercage jumps.

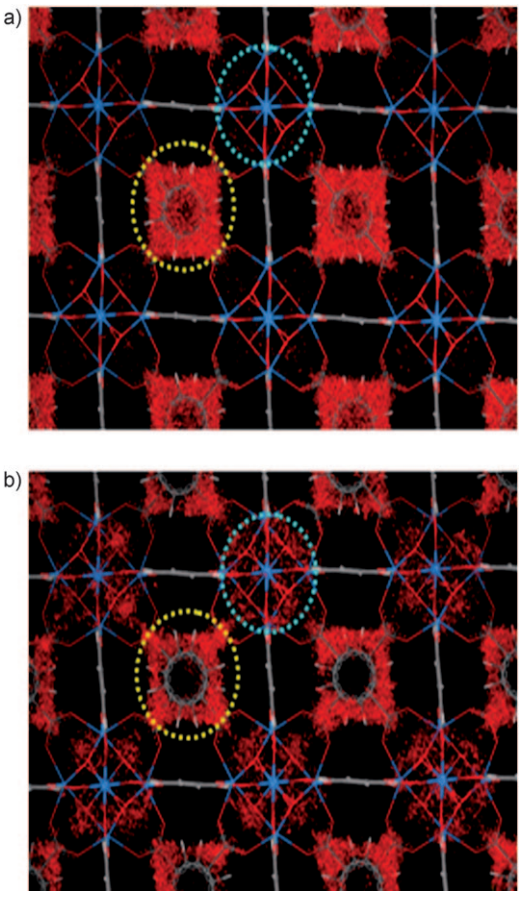

Figure 8. a) 2D probability density plots of the COM of CO_2 in UiO-66(Zr) at 230 K from MD simulations at different loadings. a) Low (7 CO_2/u.c.) and b) high loading (36 CO_2/u.c.). (Yellow and blue circles denote the tetrahedral and octahedral cages, respectively)

Conclusion

A combination of QENS measurements and MD simulations was successfully employed to probe the dynamics of CH_4 and CO_2 in MOF-type material UiO-66(Zr). The experimental self-diffusivity of CH_4 shows a maximum with increasing loading, while the measured transport diffusivity of CO_2 shows a monotonously increasing trend within the experimental concentration domain. The MD simulations based on a flexible force field for describing the framework capture very well the magnitude and profile for both D_s-(CH_4) and D_t(CO_2). They further show that these diffusion profiles observed for CH_4 and CO_2 can be well correlated with the residence time spent by the diffusive species in the tetrahedral cages. The unusual higher diffusivity of CH_4 compared to CO_2 is opposite to the trend previously observed in narrow-window zeolites. A global diffusion mechanism disclosed by MD simulations shows that both diffusive species show 3D-type diffusion behavior, in agreement with experiment, and involve a combination of intracage diffusion and jumps form tetrahedral to octahedral to tetrahedral cages.

Experimental Section

Synthesis: UiO-66(Zr) was prepared from a large-scale mixture of $ZrCl_4$, terephthalic acid, hydrochloric acid, and dimethylformamide in the ratio 25 mmol:50 mmol:50 mmol:150 mL. The slurry was then introduced into a 750 mL Teflon liner, which was inserted into a metal Paar bomb. The system was then heated for 16 h at 220 °C. The resulting white product was filtered off, washed with DMF to remove the excess of unconverted terephthalic acid, washed with acetone, and dried at room temperature. The sample was finally calcined at 250 °C under vacuum (5 mbar) to remove DMF from the framework.

QENS measurements: Since scattering from CO_2 is weak, a deuterated analogue of UiO-66(Zr) was prepared to reduce the scattering from the MOF framework. The synthesis was performed according to our previous procedure[11] with deuterated instead of hydrogenated terephthalic acid as reactant.[14] The UiO-66(Zr) sample was activated by pumping at 473 K, and final pressure was better than 10^{-3} Pa after cooling. The degassed MOF was transferred in a glovebox into a slab-shaped aluminum

container, which was connected to a gas-inlet system allowing in situ adsorption. After recording the scattering of the empty material, different loadings of CO_2 were investigated at 230 K, and the adsorbed amounts were determined by volumetry. After these runs, CO_2 was evacuated by pumping the cell at 370 K. After desorption, it was checked that the signal of the degassed MOF was identical to that of the original UiO-66(Zr) solid. Methane was then measured at various concentrations at 230 K. On IN6, the incident neutron energy was set to 3.12 meV, corresponding to a wavelength of 5.12 Å. After scattering by the sample, the neutrons are analyzed as a function of flight time and angle. The wavevector transfer Q varies with scattering angle and ranged from 0.25 to 1.2 $Å^{-1}$. Different spectra were grouped to obtain satisfactory counting statistics. Detectors corresponding to the Bragg peaks of UiO-66(Zr) were avoided as much as possible, but dehydroxylation of this MOF lowers the space group, so that elastic intensity was found at low Q. Time-of-flight spectra were converted to energy spectra. The elastic energy resolution was measured with a vanadium standard, and it could be fitted by a Gaussian function with a half-width at half-maximum varying from 40 μeV at small Q to 50 μeV at large Q.

Molecular dynamics simulations: Molecular dynamics simulations were performed by using DL_POLY 2.20 in the NVT ensemble with time step of 1 fs. The Nosé–Hoover thermostat was used to maintain the system temperature. For the current studies, the intermolecular interactions between adsorbates as well as adsorbate–adsorbents were represented by a combination of short-range van der Waals (LJ) and long-range Coulombic interactions. The former were estimated by using a cutoff radius of 14 Å, and the latter were calculated by the Ewald summation methodology. The simulation box consisting of 18 unit cells of UiO-66(Zr) and periodic boundary conditions were applied in all three dimensions. The adsorbate molecules were first loaded into the UiO-66(Zr) structure by means of Monte Carlo simulations, and the resulting configurations were equilibrated with 1×10^6 MD steps, followed by the production run of 2×10^7 MD steps (i.e., 20 ns). Further information on the force fields, partial charges of the framework atoms in MOFs, and more details of the MD simulations can be found in the Supporting Information.

Acknowledgements

The research leading to these results has received funding from the European Community's Seventh Framework Programme (FP7/2007-2013) under grant agreement no 228862". We thank Dr. M. M. Koza for his help during the measurements on the IN6 spectrometer at the Institut Laue Langevin, Grenoble, France.

[1] a) D. M. D'Alessandro, B. Smit, J. R. Long, *Angew. Chem.* **2010**, *122*, 6194; *Angew. Chem. Int. Ed.* **2010**, *49*, 6058; b) S. R. Venna, M. A. Carreon, *J. Am. Chem. Soc.* **2010**, *132*, 76.

[2] a) G. Férey, *Chem. Soc. Rev.* **2008**, *37*, 191; b) H. Li, M. Eddaoudi, M. O'Keeffe, O. M. Yaghi, *Nature* **2004**, *427*, 523; c) M. Kondo, S. Furukawa, K. Hirai, S. Kitagawa, *Angew. Chem.* **2010**, *122*, 5455; *Angew. Chem. Int. Ed.* **2010**, *49*, 5327; d) S. Bourrelly, P. L. Llewellyn, C. Serre, F. Millange, T. Loiseau, G. Férey, *J. Am. Chem. Soc.* **2005**, *127*, 13519.

[3] a) A. G. Wong-Foy, A. J. Matzger, O. M. Yaghi, *J. Am. Chem. Soc.* **2006**, *128*, 3494; b) Y. Li, R. T. Yang, *J. Am. Chem. Soc.* **2006**, *128*, 726; c) M. Latroche, S. Surblé, C. Serre, C. Mellot-Draznieks, P. L. Llewellyn, J. Lee, J.-S. Chang, S. H. Jhung, G. Férey, *Angew. Chem.* **2006**, *118*, 8407; *Angew. Chem. Int. Ed.* **2006**, *45*, 8227; d) L. J. Murray, M. Dincă, J. R. Long, *Chem. Soc. Rev.* **2009**, *38*, 1294–1314; e) X. B. Zhao, B. Xiao, A. J. Fletcher, K. M. Thomas, D. Bradshaw, M. J. Rosseinsky, *Science* **2004**, *306*, 5698.

[4] a) S. Ma, D. Sun, J. M. Simmons, C. D. Collier, D. Yuan, H.-C. Zhou, *J. Am. Chem. Soc.* **2008**, *130*, 1012; b) M. Eddaoudi, J. Kim, N. Rosi, D. Vodak, J. Wachter, M. O'Keeffe, O. M. Yaghi, *Science* **2002**, *295*, 469; c) S.-I. Noro, S. Kitagawa, T. M. Kondo, K. Seki, *Angew. Chem.* **2000**, *112*, 2161; *Angew. Chem. Int. Ed.* **2000**, *39*, 2081; d) S. Irena, S. Kaskel, *Microporous Mesoporous Mater.* **2008**, *112*, 108.

[5] a) A. R. Millward, O. M. Yaghi, *J. Am. Chem. Soc.* **2005**, *127*, 17998; b) P. L. Llewellyn, S. Bourrelly, C. Serre, A. Vimont, M. Daturi, L. Hamon, G. D. Weireld, J.-S. Chang, D.-Y. Hong, Y. K. Hwang, S. H. Jhung, G. Férey, *Langmuir* **2008**, *24*, 7245; c) H. Furukawa, N. Ko, Y. B. Go, N. Aratani, S. B. Choi, E. Choi, A. ö. Yazaydin, R. Q. Snurr, M. O'Keeffe, J. Kim, O. M. Yaghi, *Science* **2010**, *329*, 424.

[6] a) L. Bastin, P. S. Bárcia, E. J. Hurtado, J. A. C. Silva, A. E. Rodrigues, B. Chen, *J. Phys. Chem. C* **2008**, *112*, 1575; b) P. D. C. Dietzel, V. Besikiotis, R. Blom, *J. Mater. Chem.* **2009**, *19*, 7362; c) L. Hamon, E. Jolimaître, G. D. Pirngruber, *Ind. Eng. Chem. Res.* **2010**, *49*, 7497.

[7] a) Y.-S. Bae, K. L. Mulfort. H. Frost, P. Ryan, S. Punnathanam, L. J. Broadbelt, J. T. Hupp, R. Q. Snurr, *Langmuir* **2008**, *24*, 8592; b) Q. Yang, C. Zhong, *ChemPhysChem* **2006**, *7*, 1417; c) R. Babarao, J. Jiang, S. I. Sandler, *Langmuir* **2009**, *25*, 5239; d) A. Martín-Calvo, E. García-Pérez, J. M. Castillo, S. Calero, *Phys. Chem. Chem. Phys.* **2008**, *10*, 7085; e) Y.-S. Keskin, T. M. van Heest, D. S. Sholl, *ChemSusChem* **2010**, *3*, 879.

[8] a) S. R. Caskey, A. G. Wong-Foy, A. Matzger, *J. Am. Chem. Soc.* **2008**, *130*, 10870; b) D. Plant, H. Jobic, P. Llewellyn, G. Maurin, *Eur. Phys. J. A* **2007**, *141*, 127.

[9] J. H. Cavka, S. Jakobsen, U. Olsbye, N. Guillou, C. Lamberti, S. Bordiga, K. P. Lillerud, *J. Am. Chem. Soc.* **2008**, *130*, 13850.

[10] a) A. D. Wiersum, E. Soubeyrand-Lenoir, Q. Yang, B. Moulin, V. Guillerm, M. Ben Yahia, S. Bourrelly, A. Vimont, S. Miller, C. Vagner, M. Daturi, G. Clet, C. Serre, G. Maurin, P. L. Llewellyn, unpublished results; b) Q. Yang, A. D. Andrew, H. Jobic, V. Guillerm, T. Devic, C. Serre, P. L. Llewellyn, G. Maurin, unpublished results.

[11] a) R. B. Rankin, J. Liu, A. D. Kulkarni, J. K. Johnson, *J. Phys. Chem. C* **2009**, *113*, 16906; b) D. Liu, C. Zheng, Q. Yang, C. Zhong, *J. Phys. Chem. C* **2009**, *113*, 5004; c) A. Sirjoosingh, S. Alavi, T. K. Woo, *J. Phys. Chem. C* **2010**, *114*, 2171; d) R. Krishna, J. M. van Baten, *Langmuir* **2010**, *26*, 8450.

[12] a) N. Rosenbach, Jr., H. Jobic, A. Ghoufi, F. Salles, G. Maurin, S. Bourrelly, P. L. Llewellyn, T. Devic, C. Serre, G. Férey, *Angew. Chem.* **2008**, *120*, 6713; *Angew. Chem. Int. Ed.* **2008**, *47*, 6611; b) F. Salles, H. Jobic, T. Devic, P. L. Llewellyn, C. Serre, G. Férey, G. Maurin, *ACS Nano* **2010**, *4*, 143; c) F. Salles, H. Jobic, A. Ghoufi, P. L. Llewellyn, C. Serre, S. Bourrelly, G. Férey, G. Maurin, *Angew. Chem.* **2009**, *121*, 8485; *Angew. Chem. Int. Ed.* **2009**, *48*, 8335.

[13] K. Barthelet, J. Marrot, D. Riou, G. Férey, *Angew. Chem.* **2002**, *114*, 291; *Angew. Chem. Int. Ed.* **2002**, *41*, 281.

[14] H. Jobic, D. N. Theodorou, *Microporous Mesoporous Mater.* **2007**, *102*, 21.

[15] a) E. Beerdsen, B. Smit, D. Dubbeldam, *Phys. Rev. Lett.* **2004**, *93*, 248–301; b) R. Krishna, J. M. van Baten, *Microporous Mesoporous Mater.* **2008**, *109*, 91; c) A. I. Skoulidas, D. S. Sholl, *J. Phys. Chem. A* **2003**, *107*, 10132.

[16] a) I. Déroche, G. Maurin, B. J. Borah, S. Yashonath, H. Jobic, *J. Phys. Chem. C* **2010**, *114*, 5027; b) J. Kärger, H. Pfeifer, M. Rauscher, A. Walter, *J. Chem. Soc. Faraday Trans. 1* **1980**, *76*, 717; c) N. Hedin, G. J. DeMartin, W. J. Roth, K. G. Strohmaier, S. C. Reyes, *Microporous Mesoporous Mater.* **2008**, *109*, 327.

[17] a) M. G. Martin, J. I. Siepmann, *J. Phys. Chem. B* **1998**, *102*, 2569; b) S. L. Mayo, B. D. Olafson, W. A. Goddard III, *J. Phys. Chem.* **1990**, *94*, 8897.

[18] a) J. A. Greathouse, M. D. Allendorf, *J. Phys. Chem. B* **2008**, *112*, 5795; b) K. Seehamart, T. Nanok, J. Kärger, C. Chmelik, R. Krishna, S. Fritzsche, *Microporous Mesoporous Mater.* **2010**, *130*, 92.

[19] a) A. García-Sánchez, D. Dubbeldam, S. Calero, *J. Phys. Chem. C* **2010**, *114*, 15068; b) A. F. Combariza, G. Sastre, A. Corma, *J. Phys. Chem. C* **2009**, *113*, 11246.

[20] R. Krishna, *J. Phys. Chem. C* **2009**, *113*, 19756.

[21] a) S. E. Jee, D. S. Sholl, *J. Am. Chem. Soc.* **2009**, *131*, 7896; b) R. Krishna, J. M. van Baten, *Sep. Purif. Technol.* **2008**, *61*, 414.

Received: December 13, 2010
Published online: June 28, 2011

